(Received 11 December 2024, Accepted 24 December 2024, Scheduled 25 December 2024)

Dual-Color Self-Synchronized Cross-Phase-Modulation Mode-Locked Fiber Laser for Coherent Anti-Stokes Raman Scattering Detection

Pu Sun[1, 2, †], Haolin Yang[1, †], Xiaer Zou[1, 3], Ke Feng[1], Ruili Zhang[2], and Sailing He[2, 3, 4, *]

[1] *Centre for Optical and Electromagnetic Research, College of Optical Science and Engineering Zhejiang University, Hangzhou 310058, China*
[2] *Zhejiang Engineering Research Center for Intelligent Medical Imaging Sensing and Non-Invasive Rapid Testing Taizhou Hospital, Zhejiang University, Taizhou 318000, China*
[3] *National Engineering Research Center for Optical Instruments, Zhejiang University, Hangzhou 310058, China*
[4] *Taizhou Agility Smart Technologies Co., Ltd., Taizhou, China*

ABSTRACT: We present a self-synchronized dual-color cross-phase-modulation mode-locked (XPM ML) fiber laser with excellent wavelength tunability and signal-to-noise ratio for coherent anti-Stokes Raman scattering (CARS) detection. Cross-phase-modulation gives rise to self-synchronization between the two-color lasers, which enables rapid wavelengths scanning as time delay of the master laser cavity is electrically adjusted. The synchronized cavity without any mode-locking elements helps to improve the mode-locking stability and resistance to environmental interference. The pump (780 nm, 18.5 ps) and Stokes (881.1–899.4 nm, 1.5 ps) pulses obtained by second harmonic generation (SHG) are then sent to a focusing lens for CARS detection for scanning Raman shift of 1470–1701 cm^{-1}). As an example of analyte, rhodium-bisphosphine complex catalyst samples are detected. This highly stable and fast-tunable two-color XPM synchronized mode-locked laser architecture has the potential for arbitrary waveband extension would greatly improve the possibility of coherent Raman scattering imaging technology from the laboratory to practical applications in e.g., biomedical detection.

1. INTRODUCTION

Coherent anti-Stokes Raman scattering (CARS), as a label-free, noninvasive, and chemically selective detection technique, has been widely used in biomedical imaging, industrial substance detection, and other fields [1–4]. In CARS detection, if a pump (ω_P) and Stokes (ω_S) field interact with the vibrational resonance of a Raman active molecule ($\omega_P - \omega_S$), a resonant anti-Stokes signal ($\omega_{AS} = 2\omega_P - \omega_S$) is generated. This signal enables chemically selective detection of unstained samples. Additionally, to match the molecular bond vibrational energy levels of the various compound samples, at least one of the excitation laser wavelengths should be tuned [5, 6].

The first implementation of CARS imaging was based on a solid-state optical parametric oscillator (OPO). However, the system is extremely complex, bulky, sensitive to environmental interference, and suffers from the time jitter, which limits its application in clinical translation. In contrast, lasers in the form of fiber are low-cost and compact systems with strong anti-interference capabilities [7, 8], which greatly improves the possibility of CARS technology from the laboratory to practical applications.

Currently, a direct way to generate tunable dual-color synchronized ultrafast pulses based on fiber lasers involves inserting an optical filter into the cavity. However the main potential risk is that this intracavity wavelength tuning loses mode-locking due to misalignment of the cavity [9]. In addition, four-wave mixing (FWM) [10–12], soliton self-frequency shift (SSFS) [13–15], and supercontinuum (SC) filtering [16–19] are commonly used. However, these methods have certain limitations. FWM mainly relies on the cavity length of the optical delay control fiber OPO to continuously adjust the signal wavelength. Its tuning speed is usually limited by the speed of the mechanical displacement stage, and the conversion efficiency is low. The SSFS must occur in a medium with negative dispersion, and its wavelength tuning is proportional to the pump power, greatly limiting the wavelength tuning accuracy. Although the supercontinuum method can produce broadband spectra covering multiple wavelength components, the power density of each spectral component is low. At the same time, during supercontinuum broadening, various nonlinear effects compete with each other, affecting the spectral coherence and hindering coherent detection.

To reduce the risk of losing mode-locking and enhance the signal-to-noise ratio, we present a novel self-synchronized dual-color ultrafast fiber laser system for CARS microscopy through cross-phase-modulation (XPM) mode-locking. The mode-locking scheme is based on periodic phase modulation induced by XPM [20, 21], which provides passive self-stabilization. By injecting an external ultrafast seed into the synchronized laser cavity, continuous wave (CW)

* Corresponding author: Sailing He (sailing@zju.edu.cn).
† P. Sun and H. Yang contribute equally to this work.

can be directly transformed into synchronized mode-locked (ML) pulses. Compared with the solution of synchronizing two mode-locked cavities [22, 23], any active or passive mode-locking elements in the cavity are eliminated, and the wavelength tuning is simply achieved by using an electrically tunable fiber delay line instead of precise matching of the filter rotation angle and cavity length. The precise and high-speed scanning of the time delay facilitates precise and fast wavelength scanning.

Most CARS detections have focused on Raman spectra in the high-frequency region (2800–3200 cm^{-1}), including the lipid-related CH2 stretching at 2845 cm^{-1} and the resonance associated with cellular proteins at 2920 cm^{-1}. These have proven effective for various biomedical applications, such as high-speed imaging of living cells and tissues [20, 23, 24]. In comparison, the low-wavenumber Raman spectral fingerprint region, particularly the high-frequency part (1500–1700 cm^{-1}), has received less attention. However, many crucial chemical bond vibrations of organic molecules are located in this region, such as C = C (alkenes, aromatic compounds), C = N (amine compounds, imine structures), and C = O (ketones, aldehydes) double bonds stretching (at 1500–1700 cm^{-1}, 1600–1680 cm^{-1}, and 1500–1800 cm^{-1}, respectively). These specific positions provide information about different types of functional groups in compounds. For biomolecules, this region also contains common spectral features associated with the vibrational modes of lipids, proteins, and nucleic acids. It includes the lipid-related C = C stretching vibration at 1650 cm^{-1}, the protein-related Amide I mode at 1650–1690 cm^{-1} (primarily C = O stretching), and the Raman bands of each nucleotide base in DNA (Adenine at 1510 cm^{-1} and 1578 cm^{-1}, Guanine at 1578 cm^{-1} and 1659–1671 cm^{-1}, Thymine and Cytosine at 1659–1671 cm^{-1}) [25–30]. Therefore, focusing on this region is expected to meet the growing demand for high-accuracy detection in biology and medicine. Additionally, these chemical bonds are prevalent in various organic molecules and polymers, making them significant for ultrafast capture and quantitative analysis in drug development, chemical products, polymers, environmental monitoring and food safety testing [4, 31–35].

In this paper, we demonstrate a novel self-synchronized dual-color XPM ML fiber laser system with high signal-to-noise ratio and excellent capability of wavelength scanning for CARS detection. The system consists of an all-fiber Er-doped oscillator mode-locked by SESAM and an all-fiber Tm-doped self-synchronized ML oscillator without any external mode-locking elements and polarization controllers (PCs). The output is divided in two branches: the Er-doped ML laser with a repetition rate of $\sim$ 24 MHz and a pulse width of 18.5 ps is amplified and frequency doubled to 780 nm as pump branch; the other branch is Tm-doped 1.7 μm all-fiberized ML laser with a widely tunable central wavelength range from 1761.2 nm to 1790.2 nm, adjusted by the time delay of the Er-doped ML cavity through the electrically tunable fiber delay line. After amplification and frequency doubling, as Stokes pulse, it combines with the pump pulse to enable CARS detection with the Raman spectroscopy from 1470 to 1701 cm^{-1}. The two beams are then sent to a detector for CARS detection of rhodium-bisphosphine complex catalyst samples. CARS spectroscopy is obtained through scanning the delayed time of the tunable delay line.

2. EXPERIMENT SETUP

The laser system is based on a key realization that the difference wavelength of the two major fiber gain media, erbium and thulium, corresponds to a wide wavenumber region of Raman spectra, where most CARS imaging is performed. Different from the prior methods of synchronized pulses generation typically seeded by noise [10–20], here, the synchronization between the dual-color picosecond (ps) laser is based on XPM with a passive self-stabilization scheme. The detailed experimental schematic of our tunable synchronization two-color ps laser is shown in Figure 1. The whole laser system includes four parts: Er-doped ultrafast laser, Tm-doped ultrafast laser, frequency doubling and CARS detection.

The Er-doped ultrafast laser, named the master laser, is mode-locked with a SESAM (Batop, SA-1550-25-2 ps) at a repetition rate of $\sim$ 24 MHz. A piece of $\sim$ 50 cm commercial single-cladding Er-doped fiber (LIEKKI Er110-4-125) is used as the gain medium. The corresponding pump source adopted a 980 nm laser diode with a maximum output power of 600 mW is coupled into the master laser cavity through a 980/1550 nm wavelength division multiplexer (WDM). The intra-cavity laser is extracted by a 20/80 output coupler (OC). To control the laser cavity length precisely, an electrically tunable delay line (General Photonics, MDL-002) with a tuning resolution of 0.001 ps and a total 560 ps tuning range is plugged into the cavity. The the walk-off effect between the master laser and the synchronized laser (Tm-doped laser) cannot be ignored. It arises from the difference in the group velocities (v_g) of Er-doped laser and Tm-doped laser. To guarantee the two-colour laser beams maintain overlap in the time domain as they co-propagate in the synchronized laser cavity, we need a wide pulse duration (t_0) of the master laser corresponding long walk-off distance ($L_{walkoff} = t_0/(1/v_{g1} - 1/v_{g2})$). Thus, we add a bandpass filter ($\sim$ 0.42 nm) to complete the Er-doped ultrafast laser, which will lead to a wide ps-scale pulse duration generation. Then, the ps pulse laser at $\sim$ 1.56 μm is amplified by cascade fiber amplifiers (EDFA1 and EDFA2). The polarization state of the 1.56 μm pulsed laser is controlled by an external PC, so that the injected 1.56 μm laser and the synchronized laser have the same polarization state. Subsequently, the amplified 1.56 μm ultrafast laser is injected into the synchronized ML oscillator through the WDM2 and almost completely exported by the WDM3 (1550/1780 nm). This exported 1.56 μm ultrafast laser with power of $\sim$ 560 mW is frequency doubled by a periodically poled lithium niobate (PPLN1) crystal (Covesion, MSHG1550 1.0-10). With a conversion efficiency of 32% at $\sim$ 99°, we obtain 780 nm pump laser for CARS with up to 180 mW average power.

The Tm-doped laser cavity, named the synchronized laser, has the same length as the master laser cavity, and uses a piece of $\sim$ 18 cm commercial Tm-doped fiber (TDF) (OFS, TmDF200) as the gain medium. Generally, Tm-doped fiber has a wide emission spectrum from 1.6 μm to 2 μm and has a typical emission at $\sim$ 2 μm. In order to shift this gain peak to the

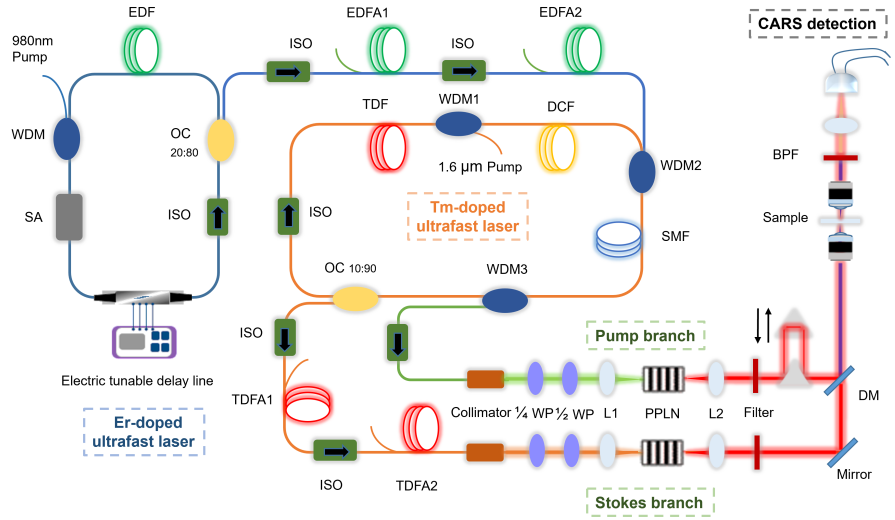

FIGURE 1. Configuration of the introduced dual-color self-synchronized cross-phase-modulation mode-locked fiber laser system. WDM: wavelength division multiplexer; EDF: Er-doped fiber; OC: optical coupler; SA: saturable absorber; ISO: polarization-insensitive isolator; DCF: dispersion compensated fiber; TDF: Tm-doped fiber; SMF: single mode fiber; WP: wave plate; PPLN: periodically poled lithium niobate; L1 and L2: lens; DM: dichroic mirror; BPF: bandpass filter.

1.7 μm waveband, a short length of TDF is necessary, which can also reduce the reabsorption at this waveband. To compensate the lower gain of short TDF, we adopt a home-built 1.6 μm laser as the pump source because of the higher absorption of TDF at this waveband than 1.5 μm waveband [36, 37]. The polarization-insensitive isolator (ISO) guarantees unidirectional propagation of the intra-cavity beams. Approximately 10% of the intra-cavity laser is extracted by a 10/90 OC. Based on the $L_{walkoff}$, a section of single-mode fiber (SMF) with length of ~ 2.34 m is used as the modulation area to realize XPM.

The injected master ultrafast laser imposes a phase change $\varphi(t)$ on the synchronized laser which corresponds to the injected pulse profile [38]. Only if the $\varphi(t)$ reaches maximum, the synchronized laser suffers the least frequency shift ($d_{\varphi(t)}$). During the circulation of the modulated synchronized laser inside cavity, only the optical component in the immediate vicinity of the zero frequency shift is retained, and ultimately form the ML pulses synchronized with the injected master laser. Therefore, the XPM-induced ML can be regarded as frequency modulation (FM) ML, which can also force the synchronized ML pulses to be stably self-synchronized with the injected master laser. When the synchronization state is disrupted by slowing the synchronized pulse train or increasing period of the injected pulse train, the center wavelength of the synchronized ML pulse train is blue-shifted, thus increasing its group velocity in the anomalous dispersion regime as well as its period. Conversely, a red-shifted center wavelength will decrease the group velocity and period of the synchronized pulse train and force the pulse train to synchronize with the injected pulse train, which provides a reliable solution for wavelength tuning [39, 40].

We splice a piece of $\sim$ 3.6 m ultrahigh numerical aperture fiber (Nefuren, UHNA4) as dispersion-compensation medium to manage the dispersion of intra cavity. The group velocity dispersion (GVD) of the UHNA4, the TDF and the SMF are $\sim$ 0.085 ps^2/m, -0.013 ps^2/m and -0.052 ps^2/m respectively [41]. The total cavity length is $\sim$ 8.5 m, corresponding to the ~ 0.059 ps^2 net cavity dispersion, showing that the laser operates in the net-normal dispersion region. The synchronized 1.7 μm ML laser is then amplified to approximately 1 W by a two-stage fiber amplifier (TDFA1 and TDFA2) and focused into PPLN2 (CTL Photonics; 10 mm period 24.74–26.22 μm) crystal at room temperature to achieve SHG as Stokes light for CARS. A bandpass filter with a center wavelength of 890 nm and a bandwidth of 30 nm is then used to remove the residual laser and high-order harmonics generation from the PPLN2 crystal. The other set of wave plates is used to adjust the polarization of the Stokes light on the sample.

3. RESULT

Figure 2 shows the optical spectra performance of the dual-color ultrafast fiber laser. The center wavelength and the spectral width measured directly from the master laser, as shown in Figure 2(a), are 1559.9 nm and 0.48 nm, respectively. The narrow spectral width of the output is derived from the sieving of 0.42 nm bandpass filter inserted in the cavity, which contributes to the improved spectral resolution. After the cascaded Er-doped fiber amplifier, 24.4 ps laser pulses with a maximum average power of $\sim$ 600 mW are obtained, which help to enhance the XPM and improve the tolerance of cavity detuning. Due to the self-phase modulation, the optical spectral broadens and splits into two peaks. The blue line depicted in Figure 2(b) illustrates that the synchronized oscillator operates at CW state with a center wavelength of 1773.3 nm, which coincides with the gain peak of the 18 cm TDF. When the electrically tunable delay line is adjusted so that the cavity length of the two oscillators is approximately the same, the 1.773 μm CW laser automatically transforms into ML laser as soon as the $\sim$ 600 mW master ultrafast laser is injected into the modulation area of the

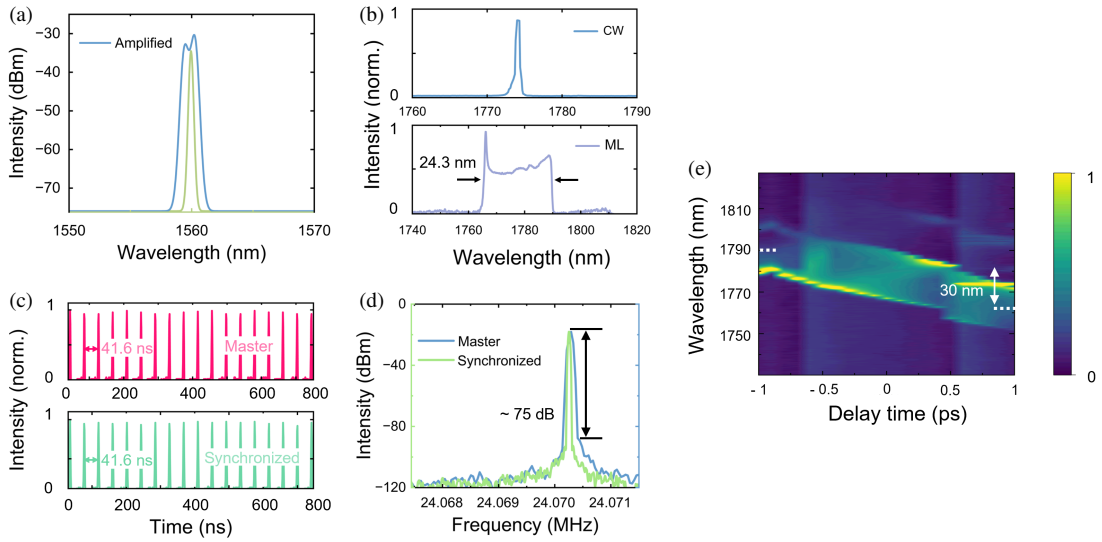

FIGURE 2. (a) Optical spectrum of the master laser (green line) and the amplified master laser (bule line). (b) Optical spectrum of the synchronized laser in CW state (bule line) and ML state (purple line). (c) Real-time pulse trains of the master and synchronized lasers at 1560 and 1773 nm, respectively. (d) RF spectra of the dual-color ultrafast lasers. (e) Tuned wavelength as the delayed time of the tunable delay line varies.

synchronized oscillator located between WDM-2 and WDM-3. As shown in Figure 2(b), the purple line depicts the ML spectrum with steep rising and falling edges, which is the sign of dissipative soliton ML laser. It can overcome the problem of limited pulse energy of solitons in anomalous dispersion laser cavities and achieve higher energy pulse output. The corresponding spectral width is ~ 24.3 nm.

As mentioned above, dual-color ultrafast laser with a close repetition rate co-propagating in one piece of fiber can be synchronized passively in the time domain due to the periodic phase modulation induced by XPM. When the period of the injected master laser is changed, the synchronized ML laser will keep synchronization state by adaptively adjusting the laser wavelength as shown in Figure 2(e). Apparently, the ML spectrum has a symmetric profile at the zero point of the cavity detuning. As adjusting the electrically tunable delay line inside the master laser cavity in two directions, the center wavelength will be blue-shifted or red-shifted, and the curve profile will gradually become asymmetric. The ML state will maintain during the adjustment until the CW laser component appears illustrating that the tolerance of cavity detuning is exceeded (± 1 ps). Ultimately, the central wavelength can be tuned continuously from 1761.2 nm to 1790.2 nm, and the tuning range and tuning accuracy are ~ 29 nm and ~ 1.5 nm (0.1 ps), respectively. Compared with the soliton self-frequency shift induced by pump power adjusting, this scheme exhibits a more powerful ability to accurately tune the laser wavelength.

Figure 2(c) depicts the real-time pulse trains of dual-color ultrafast laser, as measured by a 1 GHz bandwidth oscilloscope connected with a 10 GHz bandwidth photodetector (PD, EOT ET-5000F). the repetition period and the fundamental repetition rate are ~ 41.6 ns and ~ 24 MHz, respectively. Figure 2(d) is the narrow radio frequency spectrum of the dual-color pulses with a resolution of 10 Hz. The more accurate measured fundamental frequency are 24.070259 MHz and 24.070281 MHz with a high signal-to-noise ratio (SNR) of up to ~ 75 dB. Deviations in the resolution level of the peak position may originate from detection jitter. These results illustrate that the stable and self-synchronized dual-color ultrafast lasers we achieve.

To match the optimal wavelength window of the high-quality microscope objective lenses (Olympus) used here for focusing and highest sensitivity of the detector (typically < 1 μm), the wavelengths of the amplified dual-color ultrafast lasers are frequency-doubled. The spectrum after frequency-doubling is shown in Figure 3(a), the red line depicts the pump beam with a central wavelength of 780.1 nm and a 3 dB band width of ~ 0.8 nm, which ensures the high spectral resolution of the CARS system. The maximum output power of ~ 180 mW is finally achieved by precisely matching the operating temperature of the PPLN (372.15 K). The lines turned from green to blue represent the Stokes beam with wavelengths scanning from ~ 881.1 nm to ~ 899.4 nm, corresponding to the spectral bandwidths at different wavelengths varied from 1 nm to 2 nm. Notably, large length of PPLN has a narrow effective bandwidth, which causes the spectral narrowing phenomenon and improves the spectral resolution. The maximum average output power of ~ 90 mW can be achieved at room temperature. Figure 3(b) gives the autocorrelation traces of both the pump and Stokes beams. Assuming a Gaussian profile, the pulse widths are ~ 18.5 ps and ~ 1.5 ps, respectively, providing a reasonable compromise between signal strength and molecular sensitivity. To determine the timing jitter between the pump and Stokes pulses, the collinear beams are focused into a beta barium borate (BBO) crystal to obtain the intensity fluctuation of the sum-frequency generation (SFG) signal. As shown in inset of Figure 3(b), by precisely adjusting the delay between the two beams, a strong blue-purple SFG signal was obtained.

The pump and Stokes beams are spatially and temporally overlapped by a dichroic mirror and a free-space optical delay line. Then, the combined dual-color ultrafast lasers are coupled

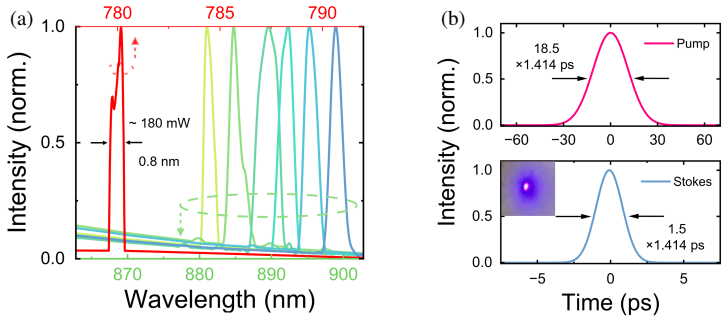

FIGURE 3. (a) Optical spectrum of the Pump (red line) and the Stokes (green-blue line) beams, the red curve corresponds to the upper wavelength axis. (b) Autocorrelation traces for the pulse widths of the pump and Stokes beams. Inset: SFG signal of the Pump and Stokes beams.

into a home-made microscope (consisted of two identical microscope objectives with numerical aperture and magnification of 0.40 and 20) for focusing into the chemical sample to be analyzed. After removing the residual pump and Stokes beams by a short pass filter (Thorlabs, FESH0750), the CARS signal (scanning in the wavelength range of 881–889 nm; corresponding to Raman shift of 1470–1701 cm^{-1}) can be recorded by a detector. To verify the precise spectra of the Raman signal, a Raman spectrometer with resolution of 10 cm^{-1} is used.

To demonstrate the unique capabilities of dual-color ultrafast fiber lasers, we perform CARS spectroscopy of the rhodium-bisphosphine complex ($C_{46}H_{44}O_8P_2$) catalyst sample, which is commonly used to catalyze the hydroformylation of olefins and is an important method for the industrial synthesis of aldehydes. Here, we select ethyl acetate as the solvent with no overlap with the Raman spectrum of the catalyst. The average powers for the pump beam and Stokes beam at the mixed solution sample were 40 and 20 mW, respectively. As shown in Figure 4, the CARS signal of the bisphosphine ligand at Raman shift of 1637 cm^{-1} is clearly observed in the C = C double bond region, which is consistent with the measured spontaneous Raman (SR) spectrum. The spectral resolution of the CARS light is $\sim$ 16 cm^{-1}, which is consistent with $\sim$ 0.8 nm spectral width of the pump.

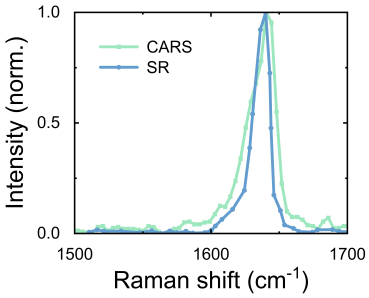

FIGURE 4. The Raman spectra fingerprint of bisphosphine measured with the present CARS system and that with spontaneous Raman (SR) detection.

4. CONCLUSION

In summary, we have demonstrated a self-synchronized dual-color XPM ML fiber laser with sufficient power and excellent wavelength tunability in the low-wavenumber region from 1470 cm^{-1}–1701 cm^{-1}, corresponding to the Stokes laser from 881.2 nm to 899.4 nm, commonly used for CARS. The fiber laser source is then used to excite the CARS signal of rhodium-bisphosphine complex catalyst samples for spectroscopic analysis. The consistency with the spontaneous Raman spectrum illustrates the reliability of this CARS detection and its applicability in material identification. Compared with several traditional synchronous tuning schemes, such as FWM, SSFS, SC, the XPM ML scheme, without the use of bandpass filters and mode-locking elements, can achieve high-accuracy and wide-range continuous tuning of the operating wavelength by simply adjusting the electrically tunable fiber delay line inside the master laser cavity. Since stable self-starting and self-synchronizing ML can be achieved without any polarization controllers inside the laser cavity, our laser source system is resistant to the environmental interference. Additionally, the scheme can be extended to a wider wavelength window (TDF: 1700 nm–2000 nm), corresponding to larger range of Raman spectroscopy, by adjusting the length of the TDF inside the cavity and using the same XPM ML method. Besides CARS detection, this stable, fast, tunable two-color fiber laser can be easily integrated with various optical imaging systems, such as any confocal microscopes with suitable detectors, to enable compact and user-friendly CARS imaging using for biomedical disease diagnosis, material analysis, and ultrafast chemical reaction kinetics.

ACKNOWLEDGEMENT

This work was supported in part by "Pioneer" and "Leading Goose" R&D Program of Zhejiang Province (2023C03083, 2023C03002, 2023C03135, 2022C03051), the Key Research and Development Program of Zhejiang Province (2021C03178), the National Key Research and Development Program of China (2022YFC3601003, 2022YFC2010000), the National Natural Science Foundation of China (W2412107, 91833303, 11621101), Ningbo Science and Technology Project (2024Z146, 2023Z179, 2021Z029, 2021Z030), Science and Technology Plan Key Project of Taizhou City (24gyz01), Science and Technology Plan Project of Luqiao (Taizhou) District (2024G2009), Ningbo Public Welfare Research Program Project (2024Z234), and the Ningbo Research Institute Project (No. 1141257B20200529). The authors are grateful to Dr. Julian Evans of Zhejiang University for valuable discussions.

REFERENCES

[1] Zumbusch, A., G. R. Holtom, and X. S. Xie, "Three-dimensional vibrational imaging by coherent anti-Stokes Raman scattering," *Physical Review Letters*, Vol. 82, No. 20, 4142, May 1999.

[2] Wei, L., Z. Chen, L. Shi, R. Long, A. V. Anzalone, L. Zhang, F. Hu, R. Yuste, V. W. Cornish, and W. Min, "Super-multiplex vibrational imaging," *Nature*, Vol. 544, No. 7651, 465–470, Apr. 2017.

[3] Virga, A., C. Ferrante, G. Batignani, D. D. Fazio, A. D. G. Nunn, A. C. Ferrari, G. Cerullo, and T. Scopigno, "Coherent anti-Stokes Raman spectroscopy of single and multi-layer graphene," *Nature Communications*, Vol. 10, No. 1, 3658, Aug. 2019.

[4] Li, H., Y. Cheng, H. Tang, Y. Bi, Y. Chen, G. Yang, S. Guo, S. Tian, J. Liao, X. Lv, S. Zeng, M. Zhu, C. Xu, J.-X. Cheng, and P. Wang, "Imaging chemical kinetics of radical polymerization with an ultrafast coherent raman microscope," *Advanced Science*, Vol. 7, No. 10, 1903644, Mar. 2020.

[5] Linnenbank, H., T. Steinle, F. Mörz, M. Flöss, H. Cui, A. Glidle, and H. Giessen, "Robust and rapidly tunable light source for SRS/CARS microscopy with low-intensity noise," *Advanced Photonics*, Vol. 1, No. 5, 055 001–055 001, Sep. 2019.

[6] Li, Y., B. Shen, S. Li, Y. Zhao, J. Qu, and L. Liu, "Review of stimulated Raman scattering microscopy techniques and applications in the biosciences," *Advanced Biology*, Vol. 5, No. 1, 2000184, Jan. 2021.

[7] Orringer, D. A., B. Pandian, Y. S. Niknafs, T. C. Hollon, J. Boyle, S. Lewis, M. Garrard, S. L. Hervey-Jumper, H. J. L. Garton, C. O. Maher, *et al.*, "Rapid intraoperative histology of unprocessed surgical specimens via fibre-laser-based stimulated Raman scattering microscopy," *Nature Biomedical Engineering*, Vol. 1, No. 2, 0027, Feb. 2017.

[8] Freudiger, C. W., W. Yang, G. R. Holtom, N. Peyghambarian, X. S. Xie, and K. Q. Kieu, "Stimulated Raman scattering microscopy with a robust fibre laser source," *Nature Photonics*, Vol. 8, No. 2, 153–159, Jan. 2014.

[9] Mashiko, Y., E. Fujita, and M. Tokurakawa, "Tunable noise-like pulse generation in mode-locked Tm fiber laser with a SESAM," *Optics Express*, Vol. 24, No. 23, 26 515–26 520, Nov. 2016.

[10] Yang, K., S. Zheng, Y. Wu, P. Ye, K. Huang, Q. Hao, and H. Zeng, "Low-repetition-rate all-fiber integrated optical parametric oscillator for coherent anti-Stokes Raman spectroscopy," *Optics Express*, Vol. 26, No. 13, 17 519–17 528, Jun. 2018.

[11] Lefrancois, S., D. Fu, G. R. Holtom, L. Kong, W. J. Wadsworth, P. Schneider, R. Herda, A. Zach, X. S. Xie, and F. W. Wise, "Fiber four-wave mixing source for coherent anti-Stokes Raman scattering microscopy," *Optics Letters*, Vol. 37, No. 10, 1652, May 2012.

[12] Gottschall, T., T. Meyer, M. Schmitt, J. Popp, J. Limpert, and A. Tünnermann, "Four-wave-mixing-based optical parametric oscillator delivering energetic, tunable, chirped femtosecond pulses for non-linear biomedical applications," *Optics Express*, Vol. 23, No. 18, 23 968–23 977, Sep. 2015.

[13] Andresen, E. R., C. K. Nielsen, J. Thøgersen, and S. R. Keiding, "Fiber laser-based light source for coherent anti-Stokes Raman scattering microspectroscopy," *Optics Express*, Vol. 15, No. 8, 4848–4856, Apr. 2007.

[14] Xie, R., J. Su, E. C. Rentchler, Z. Zhang, C. K. Johnson, H. Shi, and R. Hui, "Multi-modal label-free imaging based on a femtosecond fiber laser," *Biomedical Optics Express*, Vol. 5, No. 7, 2390–2396, Jun. 2014.

[15] Zhang, Y., J. Jiang, K. Liu, S. Wang, Z. Ma, and T. Liu, "Composite wavelength tuning for precision Raman resonance in soliton self-frequency shift-based coherent anti-Stokes Raman scattering," *Applied Physics Express*, Vol. 13, No. 9, 092002, Aug. 2020.

[16] Selm, R., M. Winterhalder, A. Zumbusch, G. Krauss, T. Hanke, A. Sell, and A. Leitenstorfer, "Ultrabroadband background-free coherent anti-Stokes Raman scattering microscopy based on a compact Er: Fiber laser system," *Optics Letters*, Vol. 35, No. 19, 3282–3284, Oct. 2010.

[17] Tu, H., Y. Liu, D. Turchinovich, M. Marjanovic, J. K. Lyngsø, J. Lægsgaard, E. J. Chaney, Y. Zhao, S. You, W. L. Wilson, B. Xu, M. Dantus, and S. A. Boppart, "Stain-free histopathology by programmable supercontinuum pulses," *Nature Photonics*, Vol. 10, No. 8, 534–540, Aug. 2016.

[18] Ozeki, Y., W. Umemura, K. Sumimura, N. Nishizawa, K. Fukui, and K. Itoh, "Stimulated Raman hyperspectral imaging based on spectral filtering of broadband fiber laser pulses," *Optics Letters*, Vol. 37, No. 3, 431–433, Feb. 2012.

[19] Yang, K., L. Huo, J. Ao, Q. Wang, Q. Hao, M. Yan, K. Huang, M. Ji, and H. Zeng, "Fast tunable all-polarization-maintaining supercontinuum fiber laser for CARS microscopy," *Applied Physics Express*, Vol. 14, No. 6, 062004, May 2021.

[20] Greer, E. J. and K. Smith, "All-optical FM mode-locking of fibre laser," *Electronics Letters*, Vol. 28, No. 18, 1741–1743, Aug. 1992.

[21] Wang, Z., S. Zheng, F. Dong, J. Wang, L. Yu, X. Luo, P. Yan, J. Wang, Q. Lue, C. Guo, and S. Ruan, "Synchronously pumped mode-locked ultrafast ytterbium-doped fiber laser," *Infrared Physics & Technology*, Vol. 125, 104302, Sep. 2022.

[22] Li, Y., K. Zhao, B. Cao, X. Xiao, and C. Yang, "Carbon nanotube-synchronized dual-color fiber laser for coherent anti-Stokes Raman scattering microscopy," *Optics Letters*, Vol. 45, No. 12, 3329–3332, Jun. 2020.

[23] Kong, C., C. Pilger, H. Hachmeister, X. Wei, T. H. Cheung, C. S. W. Lai, N. P. Lee, K. K. Tsia, K. K. Y. Wong, and T. Huser, "High-contrast, fast chemical imaging by coherent raman scattering using a self-synchronized two-colour fibre laser," *Light: Science & Applications*, Vol. 9, No. 1, 25, Feb. 2020.

[24] He, R., Y. Xu, L. Zhang, S. Ma, X. Wang, D. Ye, and M. Ji, "Dual-phase stimulated Raman scattering microscopy for real-time two-color imaging," *Optica*, Vol. 4, No. 1, 44–47, Jun. 2017.

[25] Walter, A., W. Schumacher, T. Bocklitz, M. Reinicke, P. Rösch, E. Kothe, and J. Popp, "From bulk to single-cell classification of the filamentous growing Streptomyces bacteria by means of Raman spectroscopy," *Applied Spectroscopy*, Vol. 65, No. 10, 1116–1125, Oct. 2011.

[26] Alexander, J., A. Subramanian, S. Jayaraman, and G. Ratinavel, "Raman spectroscopy for structural fingerprinting of biomolecules," *World Journal of Pharmaceutical Research*, Vol. 10, No. 13, 150–167, Oct. 2021.

[27] Potcoava, M. C., G. L. Futia, J. Aughenbaugh, I. R. Schlaepfer, and E. A. Gibson, "Raman and coherent anti-stokes raman scattering microscopy studies of changes in lipid content and composition in hormone-treated breast and prostate cancer cells," *Journal of Biomedical Optics*, Vol. 19, No. 11, 111605, Jun. 2014.

[28] Thomas Jr., G. J., "Raman spectroscopy of protein and nucleic acid assemblies," *Annual Review of Biophysics and Biomolecular Structure*, Vol. 28, No. 1, 1–27, 1999.

[29] Krafft, C., "Raman spectroscopy of proteins and nucleic acids: From amino acids and nucleotides to large assemblies," *Encyclopedia of Analytical Chemistry: Applications, Theory and Instrumentation*, 1–15, Sep. 2018.

[30] Zhang, S., Y. Qi, S. P. H. Tan, R. Bi, and M. Olivo, "Molecular fingerprint detection using Raman and infrared spectroscopy technologies for cancer detection: A progress review," *Biosensors*, Vol. 13, No. 5, 557, May 2023.

[31] Lee, Y. J., D. Moon, K. B. Migler, and M. T. Cicerone, "Quantitative image analysis of broadband CARS hyperspectral images of polymer blends," *Analytical Chemistry*, Vol. 83, No. 7, 2733–2739, Mar. 2011.

[32] Lee, Y. J., C. R. Snyder, A. M. Forster, M. T. Cicerone, and W.-l. Wu, "Imaging the molecular structure of polyethylene blends with broadband coherent Raman microscopy," *ACS Macro Letters*, Vol. 1, No. 11, 1347–1351, Nov. 2012.

[33] Ma, H., X. Han, C. Zhang, X. Zhang, X. Shi, and J. Ma, "The study of sulfonamide antibiotics in fish based on surface-enhanced Raman spectroscopy technology," *Acta Laser Biology Sinica*, Vol. 23, No. 6, 560–565, 2014.

[34] Luther, S. K., J. J. Schuster, A. Leipertz, and A. Braeuer, "Non-invasive quantification of phase equilibria of ternary mixtures composed of carbon dioxide, organic solvent and water," *The Journal of Supercritical Fluids*, Vol. 84, 146–154, Dec. 2013.

[35] Paul, A., K. Meyer, J.-P. Ruiken, M. Illner, D.-N. Müller, E. Esche, G. Wozny, F. Westad, and M. Maiwald, "Process spectroscopy in microemulsions — Raman spectroscopy for online monitoring of a homogeneous hydroformylation process," *Measurement Science and Technology*, Vol. 28, No. 3, 035502, Jan. 2017.

[36] Agger, S. D. and J. H. Povlsen, "Emission and absorption cross section of thulium doped silica fibers," *Optics Express*, Vol. 14, No. 1, 50–57, Jan. 2006.

[37] Yang, H. and S. He, "Widely tunable 1.7 µm vector dissipative soliton all-fiber thulium laser," *Journal of Lightwave Technology*, Vol. 42, No. 1, 347–353, Jan. 2024.

[38] Wegmüller, M., W. Hodel, and H. P. Weber, "Fiber laser mode-locking by pump pulse induced cross-phase modulation: A numerical analysis," *Optics Communications*, Vol. 115, No. 5-6, 498–504, Apr. 1995.

[39] Rusu, M., R. Herda, and O. G. Okhotnikov, "Passively synchronized two-color mode-locked fiber system based on master-slave lasers geometry," *Optics Express*, Vol. 12, No. 20, 4719–4724, Oct. 2004.

[40] Hsiang, W.-W., C.-H. Chang, C.-P. Cheng, and Y. Lai, "Passive synchronization between a self-similar pulse and a bound-soliton bunch in a two-color mode-locked fiber laser," *Optics Letters*, Vol. 34, No. 13, 1967–1969, Jul. 2009.

[41] He, H., M. Zhou, T. Qiao, H. M. Lai, Q. Ran, Y.-X. Ren, H. Ko, C. Zheng, K. K. Tsia, and K. K. Y. Wong, "890-nm-excited SHG and fluorescence imaging enabled by an all-fiber mode-locked laser," *Optics Letters*, Vol. 47, No. 11, 2710–2713, Jun. 2022.